

This is an Open Access document downloaded from ORCA, Cardiff University's institutional repository: <https://orca.cardiff.ac.uk/id/eprint/90851/>

This is the author's version of a work that was submitted to / accepted for publication.

Citation for final published version:

Beirne, Kathy, Rozanowska, Malgorzata and Votruba, Marcela 2016. Red light treatment in an axotomy model of neurodegeneration. *Photochemistry and Photobiology* 92 (4) , pp. 624-631. 10.1111/php.12606

Publishers page: <http://dx.doi.org/10.1111/php.12606>

Please note:

Changes made as a result of publishing processes such as copy-editing, formatting and page numbers may not be reflected in this version. For the definitive version of this publication, please refer to the published source. You are advised to consult the publisher's version if you wish to cite this paper.

This version is being made available in accordance with publisher policies. See <http://orca.cf.ac.uk/policies.html> for usage policies. Copyright and moral rights for publications made available in ORCA are retained by the copyright holders.



1 **Red Light Treatment in an Axotomy Model of Neurodegeneration**

2 Kathy Beirne ^{1,2}, Malgorzata Rozanowska ^{1,2}, Marcela Votruba ^{*1, 2,3}

3 1. School of Optometry and Vision Sciences Cardiff University, Cardiff, UK

4 2. Cardiff Institute for Tissue Engineering and Repair, Cardiff University,
5 Cardiff, UK

6 3. Cardiff Eye Unit, University Hospital of Wales, Cardiff, UK

7 *Corresponding author email: VotrubaM@cardiff.ac.uk (Marcela Votruba)

8

9 ABSTRACT

10 Red light has been shown to provide neuroprotective effects. Axotomising the optic nerve
11 initiates retinal ganglion cell (RGC) degeneration, and an early marker of this is dendritic
12 pruning. We hypothesised that 670 nm light can delay axotomy induced dendritic pruning in
13 the retinal explant. To test this hypothesis, we monitored the effects of 670 nm light (radiant
14 exposure of 31.7 J/cm²), on RGC dendritic pruning in retinal explants from C57BL/6J mice, at
15 40 minutes, 8 hours and 16 hours post axotomy. For sham-treated retinae, area under the Sholl
16 curve, peak of the Sholl curve and dendritic length at 8 hours post axotomy showed
17 statistically significant reductions by 42.3% ($p=0.008$), 29.8% ($p=0.007$) and 38.4% ($p=0.038$),
18 respectively, which were further reduced after 16 hours by 40.56% ($p<0.008$), 33.9%
19 ($p<0.007$), 45.43% ($p<0.006$), respectively. Dendritic field area was also significantly reduced
20 after 16 hours, by 44.23% ($p<0.019$). Such statistically significant reductions were not seen in
21 light-treated RGCs at 8 or 16 hours post axotomy. The results demonstrate the ability of 670
22 nm light to partially prevent *ex vivo* dendropathy in the mouse retina, suggesting that it is
23 worth exploring as a treatment option for dendropathy associated neurodegenerative diseases,
24 including glaucoma and Alzheimer's disease.

25

26 **INTRODUCTION**

27 Evidence is continually mounting in support of the potential of red and near infrared (NIR)
28 light therapy to provide protective effects in various neurodegenerative diseases including
29 Parkinson's disease and multiple sclerosis [1-3]. Red/NIR light therapy has also shown great
30 potential in the treatment of the more acute neurodegenerative conditions such as stroke, spinal
31 cord injury and traumatic brain injury [1, 4-11].

32 Since longer wavelengths have the ability to penetrate deeper than shorter wavelengths, NIR
33 light is the preferred choice for irradiating brain tissue [12]. When irradiating the retina
34 however the issue of tissue penetration, when using shorter wavelengths, is avoided.
35 Consequently, the beneficial effects of red light have been reported in the retina. Treatment
36 with 670 nm light has provided protection against cell loss in various rodent models of
37 photoreceptor damage whilst demonstrating the safety of using 670 nm light with an irradiance
38 of 60 mW/cm² on this light sensitive tissue [13, 14]. Also, 670 nm light provided protection in
39 other models retinal damage or dysfunction [15-18]. In particular, treatment with 670 nm light
40 in a rat model of partial axotomy (optic nerve transection) resulted in improved vision, 7 days
41 post injury [19].

42 Apoptosis, the primary mechanism of retinal ganglion cell (RGC) death following axotomy,
43 has been shown to be delayed until 3-4 days after axotomy, *in vivo* [20]. RGC dendritic
44 pruning, as characterized by a reduction in dendritic complexity, reduced dendritic arbor area
45 and shrinkage of dendrites, has been observed in mouse models of both glaucoma and
46 Alzheimer's disease and this event has been suggested to precede cell loss [21-23].

47 Until recently, the mechanisms by which dendrites are eliminated from the neuron were largely
48 unknown. Newly emerging data has provided some mechanistic insight into this process. The
49 findings of one such study has suggested that dendrite degeneration occurs in a process
50 independent of apoptosis involving a local loss of mitochondrial membrane potential and ATP
51 decline, which precede dendrite loss [24]. Inflammation is, likewise, thought to play a
52 prominent role in this process, as an increase in the pro-inflammatory cytokine, interferon γ ,
53 and an upregulation in complement proteins were found to be associated with the dendritic
54 pruning that occurs in neurodegenerative diseases and neural injury [25, 26]. Other findings
55 have shown the inhibition of mTOR, the key signal integrator for a variety of extracellular
56 signals including growth factors, to be involved in dendritic pruning [27]. Notably, cellular
57 stressors such as low ATP levels and inflammation have been shown to inhibit mTOR, and
58 optic nerve lesion has been shown to bring about the inhibition of an mTOR complex, an event
59 which has been shown to coincide with dendritic retraction.

60 Red/NIR light, which is absorbed by complex IV of the mitochondrial electron transport chain,
61 has been shown to upregulate the enzymatic activity of complex IV, increase the mitochondrial
62 membrane potential and increase ATP production [28-34]. Red light was also found to have an
63 anti-inflammatory effect as markers of inflammation, including complement proteins, were
64 significantly reduced in the outer retina following 670 nm light treatment [30, 31, 35-37].
65 Additionally, red/NIR light was found to modify cell growth by modulating the Akt/mTOR
66 signaling pathway in cancer cells [38]. In fact, the PI3K/Akt/mTOR pathway, which is
67 involved with cell growth, proliferation, differentiation and survival, has been reported to be
68 one of the most studied pathways that is influenced by red/NIR light [39].

69 Clearly, many of the mechanisms proposed to be involved in the dendritic pruning process are
70 potential therapeutic targets of the molecular mechanism responsible for the beneficial effects
71 of 670 nm light. Therefore, we have hypothesised that 670 nm light can delay the dendritic
72 pruning that is initiated upon axotomy. To test this hypothesis we used an *ex vivo* model of
73 dendritic pruning in the mouse retinal explant. Explanting the retina which involves axotomy
74 of the entire population of RGCs by complete severing of their axons, is rapidly followed by
75 pruning of the RGC dendrites [27]. The retinal explant, consequently, provides a platform
76 upon which to test the effects of 670 nm light on dendritic pruning in a substantially shorter
77 timeframe than would be possible in the aforementioned models of RGC degeneration. The
78 effect of 670 nm light on the RGC dendritic pruning in the retinal explant was monitored at 40
79 minutes, 8 hours and 16 hours post axotomy. Changes in RGC dendritic morphology over time
80 were investigated by employing various methods to analyze dendritic complexity, including
81 Sholl analysis, area under the Sholl curve, the maximum peak of the Sholl curve, average total
82 dendritic length and average dendritic field area.

83 **MATERIALS AND METHODS**

84 **Animals used:** Twenty five wild-type, 9 week old, male C57 BL/6J mice were used as the
85 source of retinal explants. Each mouse contributed a maximum of one retina per experimental
86 condition.

87 Mice were kept in a 12 hour light (4.88 lux of warm white fluorescent lighting with an
88 irradiance of $0.7 \mu\text{W}/\text{cm}^2$) / 12 hour light-dark cycle with food and water available *ad libitum*.

89 Maintenance and all experimental procedures were in compliance with the *ARVO Statement*

90 *for the Use of Animals in Ophthalmic and Vision Research* and were approved by the Home
91 Office, UK.

92 **Red light treatment:** Mice were killed by cervical dislocation under 275 lux of warm white
93 fluorescent light (providing total irradiance of 74 $\mu\text{W}/\text{cm}^2$ and an irradiance of 2.8 $\mu\text{W}/\text{cm}^2$ in
94 the 600-780 nm range of the electromagnetic spectrum). Retinae were then dissected under 676
95 lux of warm white fluorescent light (providing a total irradiance of 250 $\mu\text{W}/\text{cm}^2$ and an
96 irradiance of 130 $\mu\text{W}/\text{cm}^2$ in the red range). Retinae were dissected as described previously and
97 flat mounted onto a 0.4 μm pore PTFE membrane culture plate insert [40]. One retina per
98 mouse was assigned to sham treatment and the other to light treatment. The insert was placed
99 in a 6-well plate containing pre-warmed Neurobasal A media (Invitrogen) at 37 °C.

100 Red light was delivered to the retinae from a WARP 10 light source (Quantum devices, Inc.,
101 Wisconsin, USA), immediately after flat mounting. Red light-treated retinae were exposed to
102 670 ± 15 nm (half width half maximum, HWHM) light with a fluence of 31.7 J/cm², delivered
103 by 6 sequential 88 second exposures of the WARP 10 light device, over a 10 minute period, at
104 room temperature (see Supplementary Materials). Sham treated retinae were placed, at room
105 temperature, in a separate room to the light treatment. Upon cessation of the treatment, the
106 retinae were labelled using DiOlistics, either immediately or after an *ex vivo* period of 8 or 16
107 hours in a dark incubator, at 37 °C.

108 **DiOlistic labelling of retinal ganglion cells:** Retinal ganglion cells were labelled with
109 lipophilic fluorescent dyes to facilitate imaging of the RGC soma, dendrites and axon. 1,10-
110 dioleoyl-3,3,3,3 tetramethylindocarbocyanine methanesulphonate (DiO) (Invitrogen) or
111 3,3'-dihexadecyloxacarbocyanine perchlorate (DiI) coated tungsten particles were prepared

112 prior to retinal preparation, as described previously [40], which was modified from the original
113 protocol [41]. DiOlistic labelling of retinal ganglion cells and the preparation of retinae for
114 imaging was described previously [40]. Retinae were shot once at 100 psi using a Helios gene
115 gun (Bio-Rad) 3 cm from the retina through a 3 μ m pore size, high pore density cell culture
116 insert (Milipore), to deliver the dye coated particles to the RGCs. After DiOlistic labelling the
117 explants were transferred to a 5% CO₂ incubator at 37 °C for 30 minutes, to facilitate diffusion
118 of the dye throughout the cells. The retinae were fixed with 4% paraformaldehyde before
119 staining with TO-PRO nuclear stain. The retinae examined in the initial, second and third time
120 points were fixed 40 minutes, 8 hours and 16 hours, respectively, post axotomy.

121 **Analysis of RGC dendritic complexity:** RGC images were acquired with a Zeiss LSM
122 510 confocal microscope (Carl Zeiss, Ltd, UK), using a 20X (0.8 NA) objective lens, 543 nm
123 excitation and BP 565-615 nm emission filter for DiI, 488 nm excitation and BP 500-530 nm
124 emission filter for DiO and 633 excitation and 651-704 nm emission spectral window for TO-
125 PRO.

126 Images stacks were collected each 1 μ m distance along the Z-plane, from the ganglion cell
127 layer to the inner nuclear layer, producing a reconstructed 3-dimensional image. The
128 experimental groups to which the cells belonged to were masked using a Fiji plugin prior to
129 tracing [42]. Dendrites were traced using the Fiji plugin Simple Neurite Tracer [43], to
130 facilitate Sholl analysis using the automated Sholl analysis Fiji plugin. Sholl analysis [44]
131 quantitatively measures dendritic complexity, counting the number of dendritic intersections
132 with concentric rings placed at 10 μ m intervals from the soma centre to the most peripheral
133 dendrite.

134 To facilitate statistical comparison, obtaining the area under the Sholl curve for individual
135 RGCs was required. The area under the Sholl curve was obtained by integration of the area
136 under a 5 parameter Weibull curve fitted to the Sholl data of individual cells in Sigma Plot
137 using the following equation:

$$y = y_0 + a \left(\frac{c-1}{c} \right)^{\frac{1-c}{c}} * \left[\frac{x-x_0}{b} + \left(\frac{c-1}{c} \right)^{\frac{1}{c}} \right]^{c-1} * e^{-\left[\frac{x-x_0}{b} + \left(\frac{c-1}{c} \right)^{\frac{1}{c}} \right]^c} + \left(\frac{c-1}{c} \right)$$

138

139 Where a, b, c, x₀, y₀ are the fitted parameters, y is the number of intersections of dendrites with
140 concentric rings placed at 10 μm intervals from the soma centre to the most peripheral dendrite
141 and x is the distance from the RGC soma centre.

142 The total dendritic length was calculated from the sum of lengths of each dendritic path
143 measured in Simple Neurite Tracer plugin of Fiji. The dendritic field area of the RGC was
144 obtained by connecting the ends of each dendrite using a polygon tool in Fiji.

145 **Statistical analyses:** The Shapiro-Wilk test was performed in SPSS to test for normality in
146 the data. Non-parametric data were analysed using a Mann-Whitney *U* test in SPSS. *p* values
147 less of than 0.05 were considered statistically significant.

148

149 **RESULTS**

150 A total of 31 retinae out of 50 included RGCs with fluorescent labeling that allowed for
151 accurate tracing of their dendrites followed by Sholl analysis (Figure 1).

152 Sholl analysis is a method used to analyze dendritic morphology, which gives information on
153 the functionality of the neuron and its ability communicate effectively with other cells [45].

154 Since dendrites are the main regions of information input into neurons, reductions in the
155 number of dendrites could hinder the ability of the RGC to receive information from the
156 preceding bipolar and amacrine cells. Changes in dendritic morphology are associated with
157 malfunction in neurons, as seen in neurodegenerative diseases. Sholl analysis enables the
158 monitoring of these changes quantitatively by producing the data in the form of a Sholl profile.

159 In this experiment, the Sholl profile, which illustrates the number of intersections of dendrites
160 with concentric rings placed at each 10 μm distance from the cell soma, of RGCs from sham
161 treated retinæ showed a downward and leftward shift after both 8 and 16 hours *ex vivo*,
162 indicating a loss of RGC dendritic complexity over time (Figure 1C). In retinæ treated with
163 red light, the leftward shift in the RGC Sholl profile over time was less profound (Figure 1D).
164 There was a statistically significant reduction in the number of dendritic intersections at 70, 90
165 and 130 μm from the soma after 8 hours ($p<0.05$) and at 30 ($p<0.05$), 40 ($p<0.01$), 50
166 ($p<0.05$), 60-70 ($p<0.01$) and 80-110 μm ($p<0.05$) after 16 hours *ex vivo* for sham-treated
167 retinæ. In contrast, RGCs from light treated retinæ had no statistically significant reductions
168 in the number of dendritic intersections at any point on the Sholl curve after 8 or 16 hours.

169 <Figure 1>

170
171 The Sholl profile suggests that there is a difference in the area under the Sholl curve and the
172 maximum number of dendritic intersections in the Sholl plot. For statistical comparison
173 however, it was necessary to compare the Sholl profiles of the individual RGCs used to create
174 the Sholl plots in Figure 1. This was achieved by fitting a curve to the Sholl plot of each cell
175 and doing subsequent analysis using the entire population of neurons, allowing statistical
176 comparisons to be made.

177 A 5 parameter Weibull curve, fitted to each RGC, enabled the calculation of the average area
178 under the fitted curves and the average peak of the fitted curves for each experimental group
179 (Figure 2A). The average area under the fitted Sholl curves, of RGCs from sham treated retinae
180 was reduced from 2042 a.u. at 40 minutes to 1177 a.u. after 8 hours *ex vivo* ($p=0.008$) and to
181 1213 a.u. after 16 hours ($p=0.016$) (Figure 2B). For light-treated retinae the values were
182 reduced from 2186 a.u. after 40 minutes to 1804 a.u. after 8 hours and to 1706 a.u. after 16
183 hours but none of the differences were significant ($p=0.561$ and $p=0.232$, respectively) (Figure
184 2B).

185 The average maximum peak of the fitted curves for RGCs from sham-treated retinae was
186 significantly reduced from 22.1 intersections at 40 minutes to 15.5 intersections at 8 hours
187 ($p=0.007$) and to 14.6 intersections at 16 hours ($p=0.007$). In RGCs from light-treated retinae,
188 the average maximum peak of the fitted curves was reduced from 22.1 at 40 minutes to only
189 20.0 intersections after 8 hours and to 17.3 a.u after 16 hours ($p=0.639$ and $p=0.113$,
190 respectively) (Figure 2C).

191 <Figure 2>

192 The fitted curves then underwent additional analyses to explore the initial rate of branching of
193 the Sholl curve from the soma to the half maximum of the Sholl peak (Figure 3A). The initial
194 rate of branching provides information on the extent of proximal branching of the RGC
195 dendritic arbor. The rate of decay of the Sholl curve was also measured to explore the extent of
196 branching from the peak of the Sholl curve to the half maximum (Figure 3B). This parameter
197 yields information on the extent of branching occurring in the more distal region of the RGC's
198 dendritic arbor.

199 In RGCs from sham-treated retinae, there was no statistically significant change in the rate of
200 growth of the Sholl curve from the soma to the half maximum of the Sholl peak from 40
201 minutes to 8 hours (0.49 to 0.38, $p=0.125$) or from 40 minutes to 16 hours (0.49 to 0.52,
202 $p=0.910$) indicating that the branching of the most proximal dendrites was not altered up to 16
203 hours post axotomy. Similarly, changes in the rate of decay of the Sholl curve from the
204 maximum to the half maximum, in sham-treated retinae, were found not to be statistically
205 significantly different: 0.27 at 40 minutes, 0.22 after 8 hours ($p=0.170$ when compared to the
206 value at 40 minutes) and 0.20 after 16 hours ($p=0.052$ when compared to the value at 40
207 minutes) in sham-treated RGCs.

208 <Figure 3>

209 To further investigate the effects of red light on RGC dendrites after axotomy, measurements
210 of dendritic field area and total dendritic length, which are additional measures of RGC
211 dendritic complexity were obtained. Dendritic field area provides information on how widely
212 the cell spreads over the retina and relates to the size of its receptive field. Since RGCs are the
213 final neurons in the visual pathway before the light signal is transmitted to the brain, a
214 reduction in the area of the RGC dendritic field could diminish photosensitivity, impeding the
215 entire visual process. Similarly, since total dendritic length has been found to be positively
216 correlated with whole-neuron capacitance [46], a decrease in this parameter could negatively
217 impact on the ability of the cell to reach the threshold for electrical stimulation, thereby
218 reducing the likelihood of an action potential being formed.

219 The average dendritic field area for RGCs from sham-treated retinae decreased significantly
220 from 31204 μm^2 at 40 minutes to 17402 μm^2 after 16 hours *ex vivo* ($p=0.019$). Contrastingly,
221 where retinae were treated with 670 nm light, the RGCs did not experience a statistically

222 significant reduction in their average dendritic field area (28971 to 22540 μm^2 , $p=0.195$)
223 (Figure 4B).

224 A statistically significant decrease in the average total dendritic length was also seen in RGCs
225 from sham treated retinae, from 3007 μm at 40 minutes to 1851 μm at 8 hours ($p=0.038$) and
226 to 1640 μm at 16 hours ($p=0.006$). The values for dendritic length decreased from 2943 μm to
227 2430 μm after 8 hours ($p=0.286$) and 2362 after 16 hours ($p=0.170$), in RGCs that were
228 exposed to 670 nm light, but the differences were not statistically significant (Figure 5B).

229 Although the average total dendritic field area of red light-treated retinae was 30% greater than
230 in the sham-treated retinae after 16 hours, the difference was not statistically significant
231 ($p=0.385$). To determine the number of retinae required to obtain a statistically significant
232 difference between red light and sham-treated retinae after 16 hours, a sample size calculation
233 was done. It was determined that 40 additional retinae would be required for the sham-treated
234 group and 61 for the red light-treated group to achieve a statistically significant difference in
235 the dendritic field area between sham and red light-treated retinae after 16 hours at 0.8 power.

236 <Figure 4>

237 <Figure 5>

238 In summary, the statistically significant reductions in the number of RGC dendritic
239 intersections at various points on the Sholl plot were observed after 8 and 16 hours in sham-
240 treated retinae but were not seen in red light-treated retinae. Treatment with red light also
241 prevented a statistically significant reduction to the area under the Sholl curve and to the peak
242 of the Sholl curve. The results for average dendritic field area and average total dendritic
243 length measurements were consistent with Sholl analysis data, showing the ability of 670 nm
244 light to prevent statistically significant decreases in further parameters of dendritic complexity.

245 Red light prevented statistically significant reductions in the total loss of dendrites from the
246 entire RGC dendritic arbor, the total area of the dendritic field and the loss of dendrites from
247 the most densely branched region of the RGC dendritic arbor.

248

249 **DISCUSSION**

250 Herein we report, for the first time, of the ability of 670 nm light to prevent the dendritic
251 pruning that occurs upon axonal injury. In this study, we investigated the effect of 670 nm light
252 on RGC dendritic pruning which occurs in the mouse retinal explant upon axotomy of the
253 optic nerve. This degeneration was detectable by analysis of dendritic morphology after 8
254 hours and again after 16 hours, where statistically significant decreases from initial values were
255 observed in sham-treated explants. Sholl analysis revealed statistically significant reductions in
256 the number of dendritic intersections at various points of the Sholl curve after both 8 and 16
257 hours. The area under the Sholl curve, the average peak of the fitted Sholl curve, the average
258 total dendritic length and average dendritic field area after 16 hours also showed statistically
259 significant reductions from the values at 40 minutes by 40.56% ($p<0.008$), 33.9% ($p<0.007$),
260 45.43% ($p<0.006$), and 44.23% ($p<0.019$), respectively. Our results have demonstrated that
261 670 nm light can prevent the statistically significant reductions in these measurements up to 16
262 hours post axotomy, since the reductions seen in RGCs from light treated retinae were smaller
263 and not statistically significant. The results revealed that rapid intervention with 670 nm light,
264 when administered immediately after the acute optic nerve lesion, axotomy, prevented
265 significant neuronal damage.

266 Evidence has been gathered, suggestive of a role for dendritic abnormalities in the pathology
267 associated with the initial clinical symptoms of a range of neurodegenerative diseases [27].
268 Degeneration of RGCs is a hallmark of devastating retinal degenerative diseases such as
269 glaucoma and autosomal dominant optic atrophy (ADOA). A progressive degeneration of the
270 RGCs in such diseases coincides with deterioration in visual acuity, eventually resulting in
271 blindness. In experimental glaucoma, dendritic pruning has been suggested to precede selective
272 loss of RGCs [47-49]. Also in ADOA, dendritic pruning was found to begin at a time when a
273 loss in visual acuity was observed, in a mouse model of the disease [40].

274 The effect of changes to the dendritic morphology of neurons has also been observed in some
275 of the most common and debilitating, neurodegenerative diseases, including Alzheimer's
276 disease. In the postmortem brains of Alzheimer's disease patients, there was a marked decrease
277 in the number of dendritic branches in the majority of neurons from the visual and acoustic
278 cortices compared to normal controls [50]. In addition, there was a 45% decrease in the
279 dendritic field area compared with controls in these neurons. Alterations in dendritic
280 morphology has also been found in Parkinson's disease [51]. In the *substantia nigra pars*
281 *compacta* of *post mortem* tissue from Parkinson's disease patients, there was a severe
282 reduction in the dendritic length of dopaminergic type I neurons compared with healthy
283 controls [52]. Similarly, in post mortem tissue from patients with multiple sclerosis (MS), a
284 loss in dendritic arborization was observed in cortical lesions [53]. This pathology was thought
285 to contribute to the clinical symptoms of MS by decreasing the synaptic input to the cortex.
286 Since these relatively subtle changes to the neurons are thought play a role in the clinical
287 symptoms, mild beneficial effect on the survival ability of the dendrites could translate into a

288 significant clinical effect. Delaying the dendritic pruning that occurs in the early stages of these
289 neurodegenerative diseases could delay the onset of clinical symptoms, thereby providing an
290 invaluable improvement to the quality of life of patients.

291 The pathology for the initial symptoms in the discussed diseases appears to be due to a loss of
292 dendrites as opposed to cell death. Moreover, dendritic degeneration appears to occur via a
293 process independent of neuronal loss. It was found that the inhibition of pro-apoptotic proteins
294 was sufficient to delay neuronal somal death while failing to have any preventative effect on
295 dendritic pruning [54]. Therefore, looking at ways of preventing dendritic pruning may require
296 a unique approach and may also be a more fruitful treatment strategy than merely endeavoring
297 to keep dysfunctional cells alive.

298 Our understanding of the pathology of neurodegenerative diseases seems to be changing from
299 one of progressive cell loss to one whereby more subtle alterations in the dendritic morphology
300 are associated with the initial clinical symptoms. The alterations to the dendritic morphology
301 reported in the aforesaid neurodegenerative diseases were similar to those changes observed in
302 the current experiment after 16 hours post axotomy, in the retinal explant. Since rapid
303 intervention with 670 nm light treatment prevented such statistically significant alterations in
304 the dendritic morphology for up to 16 hours *ex vivo*, it is possible that it may prevent or slow
305 down the changes to the dendrites associated with the pathology of the said neurodegenerative
306 diseases.

307 **ACKNOWLEDGMENTS**

308 This study was supported by Fight for Sight, UK. We thank Nick White for help with confocal
309 microscopy and 3D image analysis. We also thank Dr. Pratyusha Ganne for her assistance with
310 retinal dissections.

311 **SUPPLEMENTARY MATERIALS**

312 Figure S1 can be found at DOI: 10.1562/2006-xxxxxx.s1.

313 **REFERENCES**

- 314 1. Naeser, M.A. and M.R. Hamblin (2011) Potential for transcranial laser or LED therapy to
315 treat stroke, traumatic brain injury, and neurodegenerative disease. *Photomedicine and laser*
316 *surgery*. 29(7), 443-446.
- 317 2. Oueslati, A., B. Lovisa, J. Perrin, G. Wagnières, H. Van Den Bergh, Y. Tardy, and H.A.
318 Lashuel (2015) Photobiomodulation suppresses alpha-synuclein-induced toxicity in an aav-
319 based rat genetic model of Parkinson's disease. *PloS one*. 10(10), e0140880.
- 320 3. Muili, K.A., S. Gopalakrishnan, J.T. Eells, and J.-A. Lyons (2013) Photobiomodulation
321 induced by 670 nm light ameliorates mog35-55 induced EAE in female C57BL/6 mice: A role
322 for remediation of nitrosative stress. *PloS one*. 8(6), e67358.
- 323 4. Fitzgerald, M., S. Hodgetts, C. Van Den Heuvel, R. Natoli, N.S. Hart, K. Valter, A.R.
324 Harvey, R. Vink, J. Provis, and S.A. Dunlop (2013) Red/near-infrared irradiation therapy for
325 treatment of central nervous system injuries and disorders. *Reviews in the Neurosciences*.
326 24(2), 205-226.

327 5. Byrnes, K.R., R.W. Waynant, I.K. Ilev, X. Wu, L. Barna, K. Smith, R. Heckert, H. Gerst,
328 and J.J. Anders (2005) Light promotes regeneration and functional recovery and alters the
329 immune response after spinal cord injury. *Lasers in surgery and medicine*. 36(3), 171-185.

330 6. Wu, Q., W. Xuan, T. Ando, T. Xu, L. Huang, Y.Y. Huang, T. Dai, S. Dhital, S.K. Sharma,
331 and M.J. Whalen (2012) Low-level laser therapy for closed-head traumatic brain injury in
332 mice: Effect of different wavelengths. *Lasers in surgery and medicine*. 44(3), 218-226.

333 7. Xuan, W., T. Agrawal, L. Huang, G.K. Gupta, and M.R. Hamblin (2015) Low-level laser
334 therapy for traumatic brain injury in mice increases brain derived neurotrophic factor (BDNF)
335 and synaptogenesis. *Journal of biophotonics*. 8(6), 502-511.

336 8. Naeser, M.A. and M.R. Hamblin (2015) Traumatic brain injury: A major medical problem
337 that could be treated using transcranial, red/near-infrared led photobiomodulation.
338 *Photomedicine and laser surgery*. 33(9), 443-446.

339 9. Dong, T., Q. Zhang, M.R. Hamblin, and M.X. Wu. Low level light in combination with
340 metabolic modulators for effective therapy. in SPIE BIOS. 2015. International Society for
341 Optics and Photonics.

342 10. Ando, T., Y-Y. Huang, and M.R. Hamblin, LLLT for stroke and brain disease. In: Hamblin
343 MR, Huang Y-Y (eds), *Handbook of photomedicine*. 2013, Boca Raton: CRC Press.

344 11. Parizotto, N.A., Y-Y. Huang, and M.R. Hamblin, LLLT for nerve and spinal cord
345 regeneration. In: Hamblin MR, Huang Y-Y (eds), *Handbook of photomedicine*. 2013, Boca
346 Raton: CRC Press.

347 12. Jagdeo, J.R., L.E. Adams, N.I. Brody, and D.M. Siegel (2012) Transcranial red and near
348 infrared light transmission in a cadaveric model. *PloS one*. 7(10), e47460.

- 349 13. Albarracin, R., R. Natoli, M. Rutar, K. Valter, and J. Provis (2013) 670 nm light mitigates
350 oxygen-induced degeneration in C57BL/6J mouse retina. *BMC neuroscience*. 14(1), 1.
- 351 14. Albarracin, R., J. Eells, and K. Valter (2011) Photobiomodulation protects the retina from
352 light-induced photoreceptor degeneration. *Investigative ophthalmology & visual science*.
353 52(6), 3582-3592.
- 354 15. Peoples, C., V.E. Shaw, J. Stone, G. Jeffery, G.E. Baker, and J. Mitrofanis (2012) Survival
355 of dopaminergic amacrine cells after near-infrared light treatment in MPTP-treated mice. *ISRN*
356 *neurology*. 2012.
- 357 16. Tang, J., Y. Du, C.A. Lee, R. Talahalli, J.T. Eells, and T.S. Kern (2013) Low-intensity far-
358 red light inhibits early lesions that contribute to diabetic retinopathy: In vivo and in vitro far-
359 red light inhibits DR. *Investigative ophthalmology & visual science*. 54(5), 3681-3690.
- 360 17. Barbosa, M., R. Natoli, K. Valter, J. Provis, and T. Maddess (2014) Integral-geometry
361 characterization of photobiomodulation effects on retinal vessel morphology. *Biomedical*
362 *optics express*. 5(7), 2317-2332.
- 363 18. Natoli, R., K. Valter, M. Barbosa, J. Dahlstrom, M. Rutar, A. Kent, and J. Provis (2013)
364 670nm photobiomodulation as a novel protection against retinopathy of prematurity: Evidence
365 from oxygen induced retinopathy models. *PloS one*. 8(8), e72135.
- 366 19. Giacci, M.K., L. Wheeler, S. Lovett, E. Dishington, B. Majda, C.A. Bartlett, E. Thornton,
367 E. Harford-Wright, A. Leonard, and R. Vink (2014) Differential effects of 670 and 830 nm red
368 near infrared irradiation therapy: A comparative study of optic nerve injury, retinal
369 degeneration, traumatic brain and spinal cord injury.

- 370 20. Magharios, M.M., P.M. D'Onofrio, and P.D. Koeberle (2011) Optic nerve transection: A
371 model of adult neuron apoptosis in the central nervous system. *Journal of visualized*
372 *experiments: JoVE*, (51).
- 373 21. Berry, R.H., J. Qu, S.W. John, G.R. Howell, and T.C. Jakobs (2015) Synapse loss and
374 dendrite remodeling in a mouse model of glaucoma. *PloS one*. 10(12), e0144341.
- 375 22. Votruba, M., P.A. Williams, R.A. Thirgood, H. Oliphant, M.A. Good, J. Williams, and J.E.
376 Morgan (2012) Retinal ganglion cell dendritic degeneration in a mouse model of alzheimer's
377 disease. *Investigative Ophthalmology & Visual Science*. 53(14), 4650-4650.
- 378 23. Williams, P.A., R.A. Thirgood, H. Oliphant, A. Frizzati, E. Littlewood, M. Votruba, M.A.
379 Good, J. Williams, and J.E. Morgan (2013) Retinal ganglion cell dendritic degeneration in a
380 mouse model of Alzheimer's disease. *Neurobiology of aging*. 34(7), 1799-1806.
- 381 24. Ikegami, K. and T. Koike (2003) Non-apoptotic neurite degeneration in apoptotic neuronal
382 death: Pivotal role of mitochondrial function in neurites. *Neuroscience*. 122(3), 617-626.
- 383 25. Kim, I.-J., H.N. Beck, P.J. Lein, and D. Higgins (2002) Interferon γ induces retrograde
384 dendritic retraction and inhibits synapse formation. *The Journal of neuroscience*. 22(11), 4530-
385 4539.
- 386 26. Stephan, A.H., B.A. Barres, and B. Stevens (2012) The complement system: An
387 unexpected role in synaptic pruning during development and disease. *Annual review of*
388 *neuroscience*. 35, 369-389.
- 389 27. Di Polo, A. (2015) Dendrite pathology and neurodegeneration: Focus on mTOR. *Neural*
390 *regeneration research*. 10(4), 559.

391 28. Karu, T. (2008) Action spectra: Their importance for low level light therapy.
392 Photobiological Sciences Online (KC Smith, editor) American Society for Photobiology,
393 <http://www.photobiology.info>.

394 29. Hamblin, M.R. and T.N. Demidova. Mechanisms of low level light therapy. in Biomedical
395 Optics 2006. 2006. International Society for Optics and Photonics.

396 30. Kokkinopoulos, I., A. Colman, C. Hogg, J. Heckenlively, and G. Jeffery (2013) Age-
397 related retinal inflammation is reduced by 670 nm light via increased mitochondrial membrane
398 potential. *Neurobiology of aging*. 34(2), 602-609.

399 31. Begum, R., M.B. Powner, N. Hudson, C. Hogg, and G. Jeffery (2013) Treatment with 670
400 nm light up regulates cytochrome c oxidase expression and reduces inflammation in an age-
401 related macular degeneration model. *PloS one*. 8(2), e57828.

402 32. Ferraresi, C., M.V.P. de Sousa, Y.-Y. Huang, V.S. Bagnato, N.A. Parizotto, and M.R.
403 Hamblin (2015) Time response of increases in atp and muscle resistance to fatigue after low-
404 level laser (light) therapy (LLLT) in mice. *Lasers in medical science*. 30(4), 1259-1267.

405 33. Ferraresi, C., N.A. Parizotto, M.V. Pires de Sousa, B. Kaippert, Y.Y. Huang, T. Koiso,
406 V.S. Bagnato, and M.R. Hamblin (2015) Light-emitting diode therapy in exercise-trained mice
407 increases muscle performance, cytochrome c oxidase activity, atp and cell proliferation.
408 *Journal of biophotonics*. 8(9), 740-754.

409 34. Karu, T., Y-Y. Huang and M.R. Hamblin, Chromophores (photoacceptors) for LLLT. In:
410 Hamblin MR, Huang Y-Y (eds), *Handbook of photomedicine*. 2013, Boca Raton: CRC Press.

411 35. Fernandes, K.P.S., N.H.C. Souza, R.A. Mesquita-Ferrari, D.d.F.T. da Silva, L.A. Rocha,
412 A.N. Alves, K. de Brito Sousa, S.K. Bussadori, M.R. Hamblin, and F.D. Nunes (2015)
413 Photobiomodulation with 660-nm and 780-nm laser on activated j774 macrophage-like cells:

414 Effect on M1 inflammatory markers. *Journal of Photochemistry and Photobiology B: Biology*.
415 153, 344-351.

416 36. Rutar, M., R. Natoli, R. Albarracin, K. Valter, and J. Provis (2012) 670-nm light treatment
417 reduces complement propagation following retinal degeneration. *J Neuroinflammation*. 9, 257.

418 37. Calaza, K.C., J.H. Kam, C. Hogg, and G. Jeffery (2015) Mitochondrial decline precedes
419 phenotype development in the complement factor H mouse model of retinal degeneration but
420 can be corrected by near infrared light. *Neurobiology of aging*. 36(10), 2869-2876.

421 38. Sperandio, F.F., F.S. Giudice, L. Corrêa, D.S. Pinto, M.R. Hamblin, and S.C. de Sousa
422 (2013) Low-level laser therapy can produce increased aggressiveness of dysplastic and oral
423 cancer cell lines by modulation of AKT/mTOR signaling pathway. *Journal of biophotonics*.
424 6(10), 839-847.

425 39. Sonis, S.T., S. Hashemi, J.B. Epstein, R.G. Nair, and J.E. Raber-Durlacher (2016) Could
426 the biological robustness of low level laser therapy (photobiomodulation) impact its use in the
427 management of mucositis in head and neck cancer patients. *Oral Oncology*. 54, 7-14.

428 40. Williams, P.A., J.E. Morgan, and M. Votruba (2010) Opa1 deficiency in a mouse model of
429 dominant optic atrophy leads to retinal ganglion cell dendropathy. *Brain*, awq218.

430 41. Gan, W.-B., J. Grutzendler, W.T. Wong, R.O. Wong, and J.W. Lichtman (2000)
431 Multicolor “Diolistic” labeling of the nervous system using lipophilic dye combinations.
432 *Neuron*. 27(2), 219-225.

433 42. Schindelin, J., I. Arganda-Carreras, E. Frise, V. Kaynig, M. Longair, T. Pietzsch, S.
434 Preibisch, C. Rueden, S. Saalfeld, and B. Schmid (2012) Fiji: An open-source platform for
435 biological-image analysis. *Nature methods*. 9(7), 676-682.

436 43. Longair, M.H., D.A. Baker, and J.D. Armstrong (2011) Simple neurite tracer: Open source
437 software for reconstruction, visualization and analysis of neuronal processes. *Bioinformatics*.
438 27(17), 2453-2454.

439 44. Sholl, D. (1953) Dendritic organization in the neurons of the visual and motor cortices of
440 the cat. *Journal of anatomy*. 87(Pt 4), 387.

441 45. Langhammer, C.G., M.L. Previtiera, E.S. Sweet, S.S. Sran, M. Chen, and B.L. Firestein
442 (2010) Automated sholl analysis of digitized neuronal morphology at multiple scales: Whole
443 cell sholl analysis versus sholl analysis of arbor subregions. *Cytometry Part A*. 77(12), 1160-
444 1168.

445 46. Gertler, T.S., C.S. Chan, and D.J. Surmeier (2008) Dichotomous anatomical properties of
446 adult striatal medium spiny neurons. *The Journal of neuroscience*. 28(43), 10814-10824.

447 47. Liu, M., L. Guo, T. Salt, and M. Cordeiro (2010) Dendritic changes in the retinal ganglion
448 cells in a rat model of experimental glaucoma. *Investigative Ophthalmology & Visual Science*.
449 51(13), 5217-5217.

450 48. Williams, P.A., G.R. Howell, J.M. Barbay, C.E. Braine, G.L. Sousa, S.W. John, and J.E.
451 Morgan (2013) Retinal ganglion cell dendritic atrophy in DBA/2J glaucoma. *PloS one*. 8(8),
452 e72282.

453 49. Pavlidis, M., T. Stupp, R. Naskar, C. Cengiz, and S. Thanos (2003) Retinal ganglion cells
454 resistant to advanced glaucoma: A postmortem study of human retinas with the carbocyanine
455 dye dii. *Investigative ophthalmology & visual science*. 44(12), 5196-5205.

456 50. Baloyannis, S. (2009) Dendritic pathology in Alzheimer's disease. *Journal of the*
457 *neurological sciences*. 283(1), 153-157.

458 51. Bertram, L. and R.E. Tanzi (2005) The genetic epidemiology of neurodegenerative disease.
459 The Journal of clinical investigation. 115(6), 1449-1457.
460 52. Patt, S., H.-J. Gertz, L. Gerhard, and J. Cervos-Navarro (1991) Pathological changes in
461 dendrites of substantia nigra neurons in Parkinson's disease: A golgi study.
462 53. Peterson, J.W., L. Bö, S. Mörk, A. Chang, and B.D. Trapp (2001) Transected neurites,
463 apoptotic neurons, and reduced inflammation in cortical multiple sclerosis lesions. Annals of
464 neurology. 50(3), 389-400.
465 54. Koike, T., Y. Yang, K. Suzuki, and X. Zheng (2008) Axon & dendrite degeneration: Its
466 mechanisms and protective experimental paradigms. Neurochemistry international. 52(4), 751-
467 760.

468 **FIGURE CAPTIONS**

469 **Figure 1:** The effect of time *ex vivo* (indicated in the graph legends) on the Sholl profiles of
470 sham (C) and light (D)-treated RGCs. Stars and daggers indicate statistically significant
471 reduction in the number of dendritic intersections, from 40 minutes to 8 hours and 16 hours,
472 respectively. To facilitate comparisons, Sholl profiles of RGCs from sham- and light-treated
473 retinas are shown at 40 minutes (A) and 16 hours (B) *ex vivo*. * $p < 0.05$, ** $p < 0.01$, † $p < 0.05$,
474 †† $p < 0.01$; Mann-Whitney *U* test. Error bars represent SEM.

475 **Figure 2:** The effect of time *ex vivo*, up to 16 hours, on the average area under the fitted
476 curves (B) and average maximum Sholl peaks (C) of sham and light treated RGCs. Stars
477 placed below means indicate statistically significant reductions from the value at 40 minutes,
478 in RGCs from sham-treated retinae. *p* values placed above the means correspond to statistical

479 comparisons made between light-treated RGCs. p values placed next to the means correspond
480 to statistical comparisons made between sham and light-treated RGCs at each time point. (A)
481 A Weibull, 5 parameter curve was fitted to the Sholl data of each individual RGC. Inset: the
482 equation used to create the curve. * $p < 0.05$, ** $p < 0.01$; Mann-Whitney U test. Error bars
483 represent SEM.

484 **Figure 3:** The effect of time *ex vivo*, up to 16 hours, on the initial rate of branching of RGC
485 dendrites (A) and the rate of decay of the Sholl curve (B). p values placed below the means
486 relate to statistical comparisons made between sham-treated RGCs. p values placed above the
487 means correspond to statistical comparisons made between light-treated RGCs. p values placed
488 next to the means correspond to statistical comparisons made between sham and light-treated
489 RGCs at each time point. Mann-Whitney U test. Error bars represent SEM.

490 **Figure 4:** The effect of time *ex vivo*, up to 16 hours, on the average dendritic field area of
491 light and sham treated RGCs. (A) The Z-projected image of an RGC showing the dendritic
492 field area measurement using a polygon tool in ImageJ. Stars placed below the means indicate
493 statistically significant reductions from the value at 40 minutes, in RGCs from sham-treated
494 retinae. Stars and p values placed above the means correspond to statistical comparisons made
495 between light-treated RGCs. p values placed next to the means correspond to statistical
496 comparisons made between sham and light-treated RGCs at each time point.. * $p < 0.01$; Mann-
497 Whitney U test. Error bars represent SEM. Arrow indicates the axon. Scale bar represents 100
498 μm .

499 **Figure 5:** The effect of time *ex vivo*, up to 16 hours, on the average dendritic field length of
500 RGCs from sham and light treated retinae. (A) A 3-D image of an RGC tracing used to
501 calculate dendritic field length measurements. (B) Stars placed below the means indicate
502 statistically significant reductions from the value at 40 minutes, in RGCs from sham-treated
503 retinae. *p* values placed above the means correspond to statistical comparisons made between
504 light-treated RGCs. *p* values placed next to the means correspond to statistical comparisons
505 made between sham and light-treated RGCs at each time point. * $p < 0.01$, ** $p < 0.01$; Mann-
506 Whitney *U* test. Error bars represent SEM. Arrow indicates the axon.

507

508

509

510

511

512

513

514

515

516

517

518

519

Figure 1

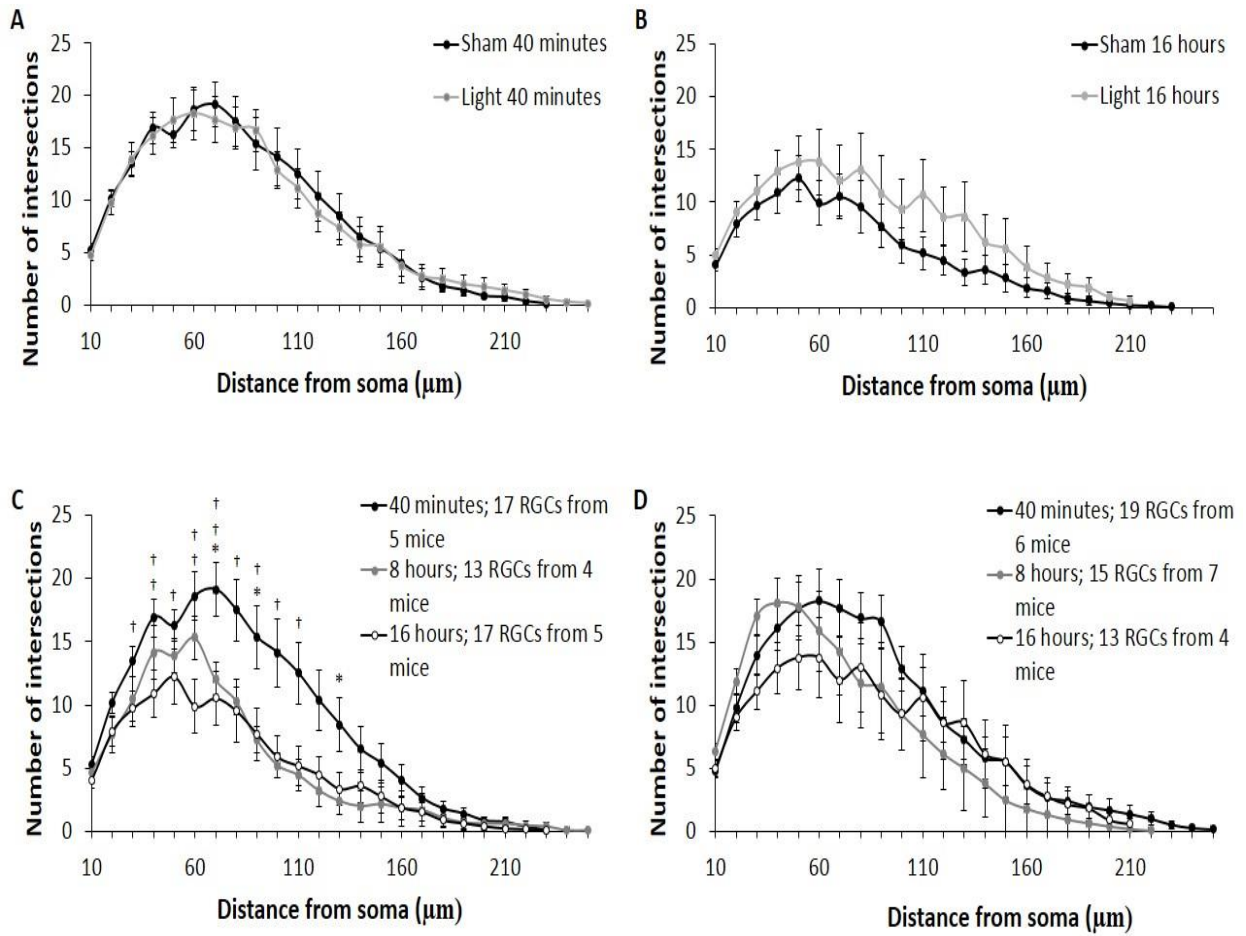


Figure 2

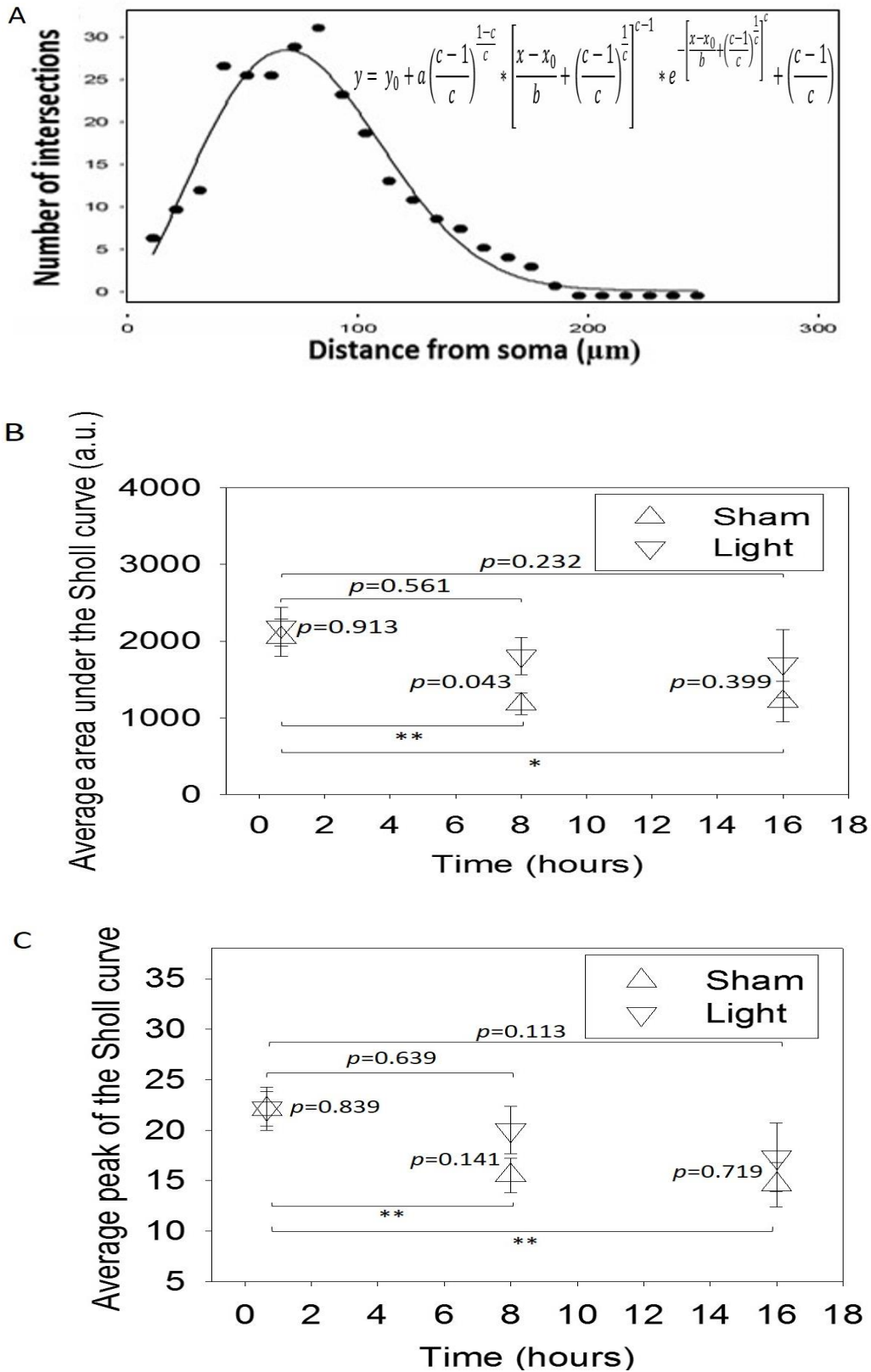


Figure 3

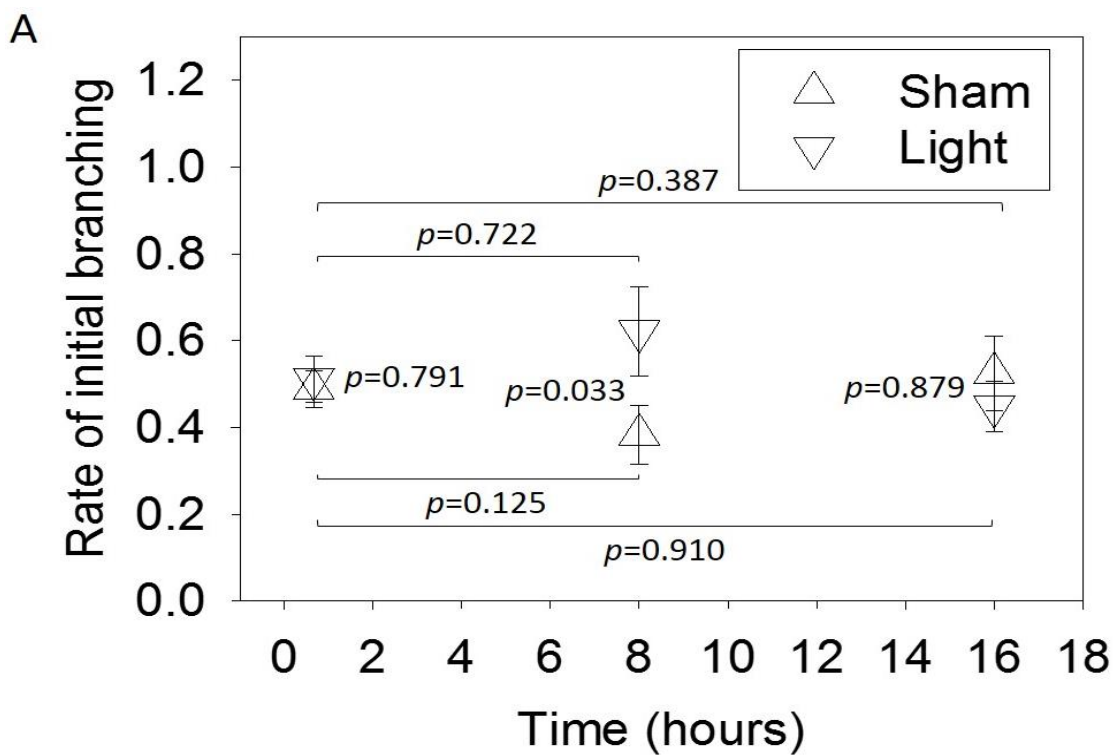
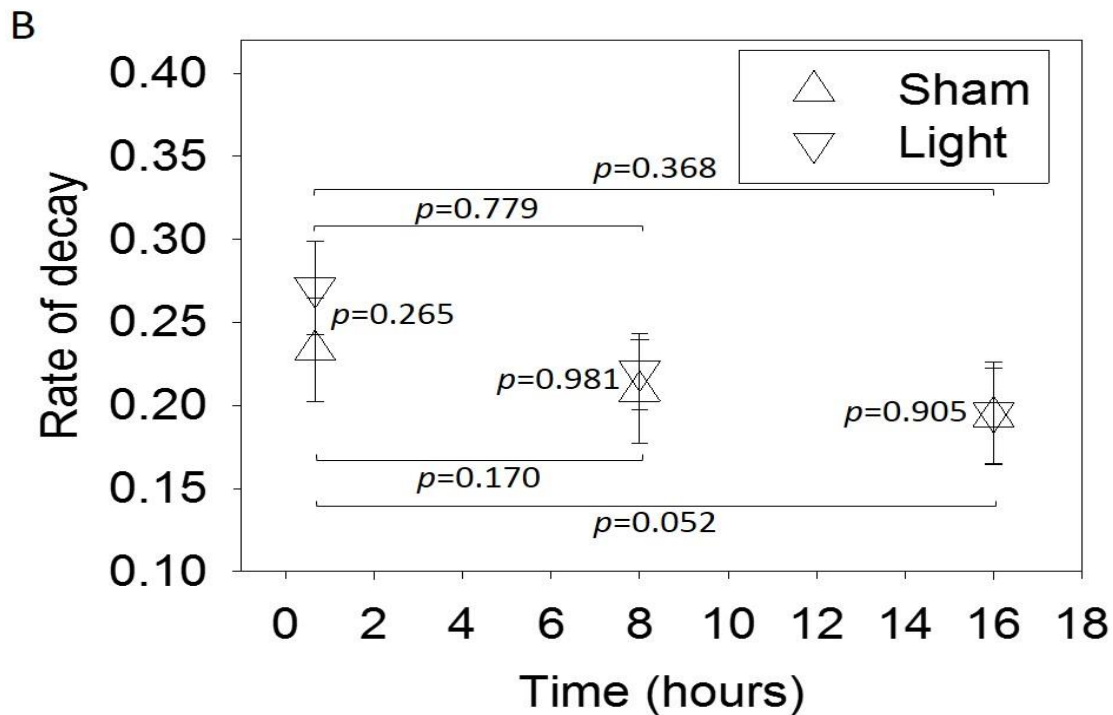
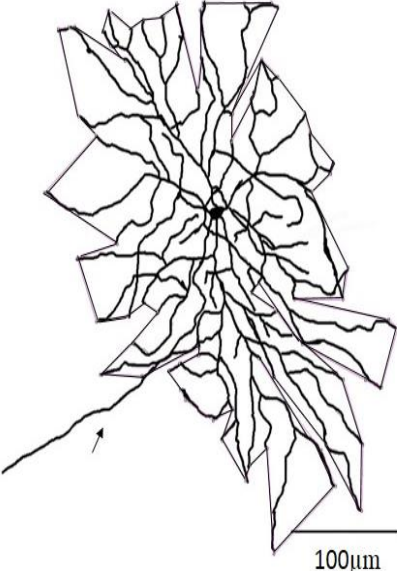


Figure 4

A



B

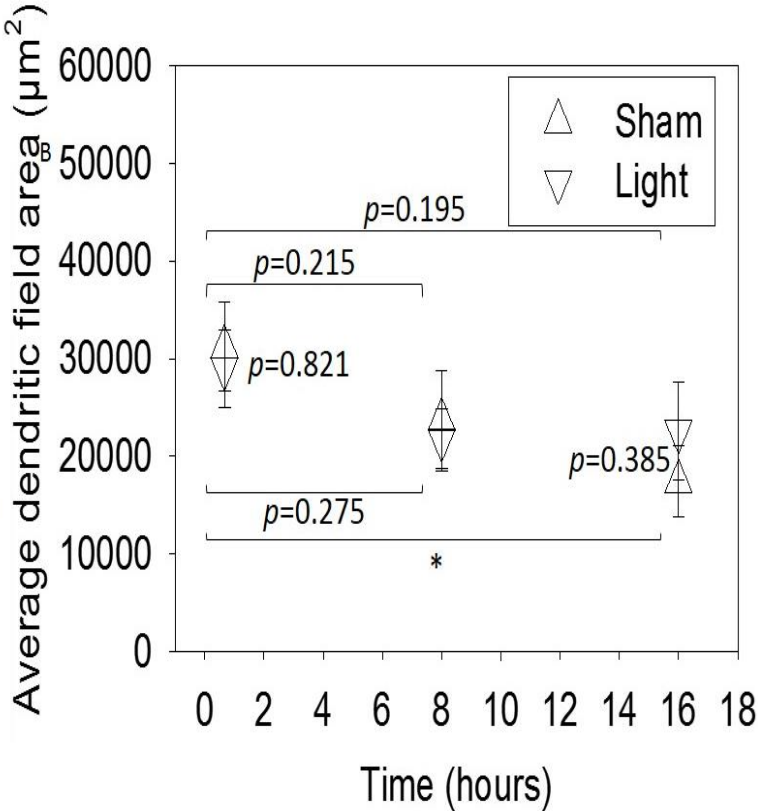
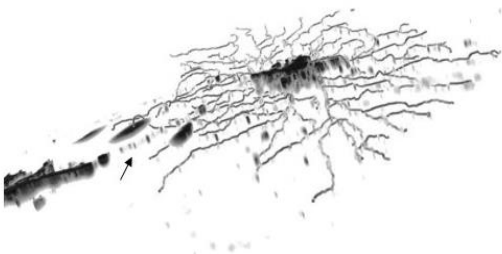


Figure 5

A



B

